Title

The Disks of Galaxies with Seyfert and Starburst Nuclei. II. Near-Infrared Structural Properties

Journal

The Astrophysical Journal, 510(2)

ISSN

0004-637X

Authors

Hunt, LK
Malkan, MA
Moriondo, G
et al.

Publication Date

1999-01-10

DOI

10.1086/306607

Peer reviewed

The Disks of Galaxies with Seyfert and Starburst Nuclei: II. Near-Infrared Structural Properties

L. K. Hunt
C. A. I. S. M. I. - C. N. R.
Largo E. Fermi 5, I-50125 Firenze, Italy
Electronic mail: hunt@arcetri.astro.it

M. A. Malkan
University of California
Department of Astronomy, 405 Hilgard Ave.,
Los Angeles, CA, U.S.A.
Electronic mail: malkan@bonnie.astro.ucla.edu

G. Moriondo
Università di Firenze
Istituto di Astronomia, Largo E. Fermi 5, I-50125 Firenze, Italy
Electronic mail: gmorio@arcetri.astro.it

and

M. Salvati
Osservatorio Astrofisico di Arcetri
Largo E. Fermi 5, I-50125 Firenze, Italy
Electronic mail: salvati@arcetri.astro.it

ABSTRACT

We have derived the near-infrared structural components of a sample of Seyfert and starburst (SBN) host galaxies by fitting the images of Hunt et al. (1997) with a new two-dimensional decomposition algorithm. An analysis of the fitted parameters shows that Seyfert 1 and SBN bulges resemble normal early-type bulges in structure and color, with $(J-K)^c_b$ about 0.1 mag redder than disk $(J-K)^c_d$. Seyfert 2 bulges, instead, are bluer than normal with $(J-K)^c_b \sim (J-K)^c_d$. Seyfert disks (especially Type 1), but not those of SBNs, are abnormally bright (in surface brightness), significantly more so than even the brightest normal disks. Seyfert disks are also compact, but similar to those in normal early-type spirals. For a given mass, Seyferts and especially SBNs are abnormally rich in neutral hydrogen, and there is strong, albeit indirect, evidence for lower mass-to-light (M/L) ratios in Seyfert and SBN *disks*, but for normal M/Ls in their bulges. In Seyferts and SBNs, HI mass fractions and M/L ratios are anticorrelated, and we attribute the high gas mass fractions and low M/Ls in SBNs and several Seyferts to

ongoing star formation. Such abundant gas in Seyferts would be expected to inhibit bar formation, which may explain why active galaxies are not always barred.

Subject headings: galaxies: Seyfert; galaxies: starburst; galaxies: active; galaxies: structure; infrared: galaxies

Accepted for publication in ApJ.

1. Introduction

While for many years, work on Seyfert activity was focussed on the properties of the active nucleus (AGN), more and more studies of Seyfert activity are now aimed at characterizing the host galaxy. Such a trend is mainly motivated by the notion that Seyfert activity, like violent star formation, needs to be maintained by a reliable supply of fuel, the source of which is thought to be in the galactic disk. Recent theoretical work, for example, has shown that non-axisymmetric potentials, such as bars, are effective movers of gas into the central potential well, thus providing a mechanism for feeding the Seyfert nucleus (Norman 1987; Shlosman, Begelman, & Frank 1989; Barnes & Hernquist 1991). Such non-axisymmetric potentials could be induced by galactic encounters (e.g., Hernquist 1989), or by cool disks, unstable to perturbations (Heller & Shlosman 1994).

The putative overabundance of bars in Seyferts is, however, still a subject of controversy. Some statistical work suggests that Seyfert nuclei are more prevalent in barred galaxies (Arsenault 1989), but other authors conclude that the frequency of bars in Seyfert hosts is the same as that in normal spirals (Moles, Marquez, & Perez 1995). Observational studies of Seyferts have found no excess of bars relative to normal galaxies (McLeod & Rieke 1995; Ho, Filippenko, & Sargent 1997; Mulchaey & Regan 1997). Moreover, when the centers of Seyfert galaxies are examined at high resolution, there is still no evidence that either inner bars or double/multiple nuclei are unusually common (Malkan, Gorjian, & Tam 1998).

Interactions in Seyfert galaxies are subject to a similar controversy. While many studies find a connection between interactions and Seyfert activity (Dahari 1985; Keel et al. 1985; Fuentes-Williams & Stocke 1988; Rafanelli et al. 1995), AGNs are also found in isolated galaxies (Moles et al. 1995; Keel 1996). Moreover, it appears that Seyfert activity is virtually absent in very disrupted systems (Keel et al. 1985; Bushouse 1987).

Recent work on the connection between environmental factors and nuclear activity has also concentrated on the properties of the bulge (e.g., Nelson & Whittle 1995). Seyfert nuclei tend to reside preferentially in early-type spirals (e.g., Moles et al. 1995), and intuitively the bulge would be expected to be connected with the properties of the central gravitational potential well. If massive compact objects (black holes) lie at the heart of Seyfert activity (c.f., Terlevich et al. 1992), the importance of the bulge can be appreciated by considering the correlation of putative black hole mass with the mass of the bulge (Kormendy & Richstone 1995). The relative dominance of the bulge in a galaxy may also be connected with the size and strength of a bar, and with the locations of resonances where gas piles up and star formation ensues (Elmegreen & Elmegreen 1985; Combes & Elmegreen 1993).

In this paper, we study both structural components of Seyfert host galaxies by decomposing the two-dimensional images into a bulge and a disk. In an earlier paper (Hunt et al. 1997, hereafter Paper I), near-infrared (NIR) images of galaxies with Seyfert and starburst nuclei (SBN) were used to quantify the host galaxies in terms of stellar populations. We found that both Seyfert and SBN host galaxies have NIR colors that reflect, in the mean, normal late-type stellar populations. We also found non-axisymmetric red colors primarily in SBNs and blue colors in Seyfert 2s, which could be interpreted as a (possibly evolutionary?) sequence from SBNs, to Type 2, to Type 1 Seyferts. Here, we have decomposed the NIR images in Paper I into bulge and disk components, and have compared their structural parameters and component colors with those from normal spirals. In §2, we briefly describe the Seyfert and SBN samples introduced in Paper I, together with the control samples of normal spirals to which we applied the same decomposition algorithm. The image decomposition is described in §3, and the structural parameters of Seyfert and SBN bulges and disks are given in §4, and compared with those of normal galaxies in §5. Implications of our results are discussed in §6. We defer analysis of the non-axisymmetric features of Seyfert galaxies to a much larger sample (Hunt et al., in preparation), and discussion of the nuclear amplitudes and colors to a future paper. As in Paper I, we use a Hubble constant $H_0 = 75$ km s^{-1}Mpc^{-1}.

2. The Samples

The Seyferts studied here and in Paper I are part of the CfA sample (Huchra & Burg 1992), and the SBNs were selected from the Markarian lists as identified and compiled by Balzano (1983) and Mazzarella & Balzano (1986). Both samples are magnitude-limited, and we imposed a redshift constraint of $z \geq 0.015$ to ensure compatibility with detector field-of-view. The

selection criteria and observations are described in detail in Paper I where J-, H-, and K-band images of 26 Seyfert 1s, Seyfert 2s, and SBNs are presented. One of the SBNs, Mrk 732, is, in reality, a Seyfert 1 (Osterbrock & Pogge 1991), and has therefore been included as a Seyfert in the statistical analysis.

Besides these "active" objects, two additional normal spiral samples for which we have NIR images have also been considered in this paper. The first is selected from the normal spiral galaxies described in de Jong & van der Kruit (1994) and in de Jong (1995), and is a minimum-diameter-limited sample. This data set was also used as a control sample in Paper I, and as mentioned there, we used only those objects with well-defined spiral types between Sa and Sc, and the same selection criteria as for the program samples were applied, that is to say $z \geq 0.015$. The subset of the de Jong galaxies (hereafter referred to as "Sc's") considered here and in Paper I is dominated by later spiral types; only two galaxies have a morphological type earlier than Sb, and most are clustered around Sc. One of the "Sc's" is Mrk 545 (UGC 89, NGC 23), a SBN, and was eliminated from consideration in the statistical comparison.

The second normal galaxy sample comprises the early-type spirals studied in Moriondo, Giovanardi, & Hunt (1998a, 1998b; hereafter MGH1, MGH2). These galaxies are taken mainly from the work of Rubin and collaborators (Rubin et al. 1985) who selected Sa's from Sandage & Tammann (1981). They are relatively luminous systems with dominant bulges; the observing sample reported in MGH1 contains only those galaxies with apparent diameter $\lesssim 4$ arcmin. The morphological type spread in this sample is tight with only one galaxy (NGC 5879) as late as Sbc, and the remaining objects are Sab or earlier. The Moriondo (hereafter referred to as "Sa's") and de Jong samples together span the entire range of spiral types, with early-types well represented for comparison with the Seyferts.

We anticipate here the sample medians for K-band galaxy total luminosity: the medians are, in descending order, -24.5 (Sy 1's), -24.3 (Sc's), -24.2 (Sa's), -23.9 (Sy 2's), and -23.8 (SBNs). The samples are similar in luminosity, and, moreover, the spread for each sample is also similar and relatively small, about 3 mag. Therefore, we do not expect to find luminosity-dependent biases in the derived structural parameters.

3. Galaxy Decomposition

Previous studies of Seyfert galaxies that examined the host galaxy bulge and disk relied on the decomposition of one-dimensional (1D) surface brightness (SB) profiles (Yee 1983; MacKenty 1990; Kotilainen et al. 1992; Danese et al. 1992)[1]. Such techniques generally fail to provide reliable galaxy structural parameters (Byun & Freeman 1995). This can be understood by considering the general case of a system inclined relative to the plane of the sky. When a galaxy is inclined, projected bulge and disk components have quite different shapes, and their sum is not well-represented by elliptical isophotes. Hence, even if the galaxy would be well-described by the simple two-component bulge+disk model, it is difficult if not impossible for 1D profile-fitting to estimate correctly the true parameters (Burstein 1979).

We have therefore adopted a technique which fits two-dimensional (2D) surface brightness distributions as the sum of a bulge, a disk, and an unresolved point source. The bulge, assumed to be an oblate rotational ellipsoid coaxial with the disk, is modelled with a generalized exponential (Sèrsic 1968, Sparks 1988):

$$I_b\,(x,y) \;=\; I_e \exp\left\{-\alpha_n\left[\left(\frac{1}{r_e}\sqrt{x^2+\frac{y^2}{(1-\epsilon_b)^2}}\;\right)^{1/n}-1\right]\right\} \tag{1}$$

Bulge index $n = 4$ corresponds to the "standard" $R^{1/4}$ law. I_e (μ_e in magnitude units) and r_e are effective (half-light) surface brightness and radius, ϵ_b is the apparent bulge ellipticity, and α_n is a constant relating the effective brightness and radius to the exponential values (see MGH1). The bulge apparent eccentricity e_b is related to the intrinsic eccentricity e'_b by:

$$e_b = e'_b \sin\, i \;\;. \tag{2}$$

The disk, assumed to be thin, is modelled with a simple exponential:

$$I_d\,(x,y) \;=\; I_d(0) \exp\left[-\frac{1}{r_d}\sqrt{x^2+\frac{y^2}{\cos^2\, i}}\;\right] \;. \tag{3}$$

$I_d(0)$ (μ_d in magnitude units) and r_d are the central surface brightness and exponential folding length, respectively, and i is the system inclination. The unresolved nuclear source is assumed to be a delta function with amplitude $I_n(0)$ (m_n in magnitude units).

[1] Yee and MacKenty applied a single-component disk model.

Structural parameters were determined by fitting the model, convolved with a circular Gaussian PSF, to the data in flux units using a χ^2 minimization. Weights were assigned to each pixel according to the photon noise expected in background-limited performance, behavior that was verified observationally. For each galaxy, the bulge was fit with four values of the exponent n: 1, 2, 3, and 4. Because the field-of-view of IRCAM1 is relatively small, there are rarely stars in the same image as the galaxy. Hence, the seeing width σ was determined by fitting a circular Gaussian to standard stars taken close in time to the program objects. The galaxy center was determined by applying Gaussian fits to the images, and the position angle of the galaxy on the sky was determined when possible from NED[2], or otherwise from the images themselves.

The algorithm fits three parameters for the bulge (I_e, r_e, and ϵ_b), three for the disk ($I_d(0)$, r_d, i), and one for the nucleus ($I_n(0)$). Because we saw no evidence for changes in scale length with wavelength, and because simulations demonstrated that parameters are generally more reliable when more than one wavelength is fit simultaneously, each galaxy was fit using all of the available images in different filters. The bulge and disk scale lengths, r_e and r_d, are therefore assumed to be the same for all wavebands, as are bulge ellipticity e_b and system inclination i. For three bands, then, there are 13 free parameters in the fit. Bulge index n is not free to vary, as mentioned above, so that the value of n that gave the best overall fit, n_{best}, was chosen a posteriori. The fitting routine is described in detail in MGH1.

One feature of the decomposition used here bears special mention. Before fitting, the galaxy image is folded about its major and minor axes to generate only one quadrant. Such a procedure is possible because of the axial symmetry of the model. The uncertainty for each point is calculated as the maximum of the photon noise, as mentioned above, and the deviations from symmetry measured in the folding process. When bars, oval distortions, or other asymmetric structures are not coincident with the line of nodes, such deviations are much larger than the photon statistical uncertainties, and those regions are therefore fit with lower weight than more symmetric ones. Hence, sensitivity to non-axisymmetric structures is much reduced, relative to a more conventional fitting technique, making the algorithm less subject to confusion between bars or lenses and bulges or disks.

[2]The NASA/IPAC Extragalactic Database (NED) is operated by the Jet Propulsion Laboratory, California Institute of Technology, under contract with the U.S. National Aeronautics and Space Administration.

3.1. Numerical Simulations

The problem of separating the nucleus in active galaxies from the bulge does not have a simple solution. To assess how well our algorithm succeeds in this task, in addition to the simulations reported in MGH1, we fit a series of synthetic galaxies with an active nucleus, bulge, and disk components. To better approximate the NIR observing conditions, we added background and photon noise typical of those in our images. J, H, and K images were synthesized for each simulation, convolved with an appropriate PSF, then fit using the same procedure as for the program galaxies.

Our main concern was the accuracy of bulge parameters when r_e is comparable with the seeing σ. Hence, for all synthetic galaxies, we fixed the disk, the nucleus, and the seeing width, and varied bulge n, e_b, r_e, and μ_e. The nucleus and the disk were chosen to have the same properties as the sample medians (disk with $r_d = 6$ arcsec, $\mu_d(K) = 17.0$, $J-K = 0.91$, $H-K = 0.20$, $i = 45°$; nucleus with $m_n(K) = 13.0$, $(J-K)_n = 1.5$, $(H-K)_n = 0.5$). The seeing FWHM was fixed to 1.6, 1.4, and 1.3 arcsec, in J, H, and K, respectively.

It turns out that the most difficult parameter to determine correctly is bulge n_{best}. This is the parameter that, in effect, describes the *shape* of the bulge; fixing n is the same as assuming homologous shapes for all bulges. If this quantity can be unambiguously determined, then the fitting algorithm returns the correct parameters of all components within the uncertainties. In general, large-n bulges are equally well fit by either $n_{best} = 3$, 4, while their small-n (1, 2) counterparts give correct (unambiguous) n_{best}. Spherical bulges with $r_e \sim \sigma_{seeing}$ are equally well fit by any n.

Perhaps the most important result of our simulations is that in all cases the disk parameters are well determined, as are the nuclear amplitudes and colors. For all simulations, independently of the correct n_{best}, we found that the fitted disk r_d and the nuclear m_n (and colors) reproduce those of the synthetic galaxies to within a few percent. Disk μ_d (and colors) are also fit to within a few percent, except for large-r_e, large-

n bulges where the fitted disk surface brightness can be wrong by as much as 0.3 mag arcsec^{-2}, although colors remain accurate.

4. Results

The major-axis cut extracted from the image together with the best-fit decomposition is shown for each program galaxy in Fig. 1. The results of our 2D decompositions are reported in Table 1. If the best-fitting bulge exponent n_{best} can be well-determined, the bulge parameters can be considered reliable. "Well-determined" means that there is a unique lowest value of χ^2 for a specific value of bulge exponent n. For one-third of each of the samples analyzed (Sy 1, Sy 2, SBN, Sa, Sc), this is not true and bulge n_{best} is "ill-determined"; thus for these objects the bulge parameters are less reliable than they would be otherwise (and are marked with a colon in Table 1).

We have checked that components are not misidentified by the decomposition algorithm. For example, bars may be mistaken for either highly-flattened bulges or disks. Since roughly half of each of the "active" samples are barred, at least as noted in de Vaucouleurs et al. (1991) – RC3 (see Paper I), this presents a potential problem. Bars are generally characterized by a large aspect ratio, and in particular, if bars are interpreted as disks by the fitting algorithm, the fitted inclinations should be larger than the "nominal" ones (those given by RC3 or measured from the outer J-band isophotes). The mean ratio of nominal to fitted inclinations for the active samples as a whole is 0.95 with a scatter of 0.5; for the Seyfert 1 sample alone the ratio is 0.89. It appears that the fitted inclinations do not differ systematically from the "nominal" ones. We conclude, albeit tentatively, that the "disks" given by the decomposition really are the photometric structures normally called disks. Mis-identification of bars for bulges is more difficult to check, since we have no way of determining, a priori, the intrinsic ellipticity of a given bulge. Nevertheless, only Mrk 545 (SBN) has a fitted bulge with e_b (0.45) which exceeds expected ranges of oblate ellipsoids (Mihalas & Binney 1981).

The fitted parameters for each of the samples are shown as histograms in Fig. 2. Table 2 gives the individual sample medians for all of the fitted parameters.

Typical Seyfert and SBN bulges are similar, being relatively spherical, compact, and bright, with $r_e \sim 1$ kpc and $\mu_e^c(K) \sim 16$ mag arcsec^{-2}. They tend to differ only in the bulge exponent n_{best}, or "shape parameter", with Seyferts having $n_{best} \sim 2$–3, and SBNs having $n_{best} \sim 1$. Seyfert 1 bulges appear to be the most luminous, with $M_b(K) \sim -23.5$.

The typical Seyfert disk is also compact and bright, with $r_d \sim 2$ kpc, and $\mu_d^c(K)$ of around 16.7 mag arcsec^{-2}. SBN disks are slightly more extended and faint, and appear similar to early-type disks, with $r_d \sim 2.8$ kpc, and $\mu_d^c(K) \sim 17.3$ mag arcsec^{-2}. Seyfert disks are also luminous, especially those of Seyfert 1s, with a median $M_d(K) \sim -24.2$.

4.1. Bulge and Disk Colors

As foreseen in Paper I, disk colors $(J-K)_d^c$ and $(H-K)_d^c$ of the active samples are similar to those in normal spirals. Furthermore, as in most spirals (MGH1), bulge $(J-K)_b^c$ of all the galaxies *except the Type 2 Seyferts* are $\sim$ 0.1 mag redder than disk $(J-K)_d^c$. In particular, Sa bulges are significantly (97% one-tailed) redder than their disks. On the other hand, Seyfert 2 bulges tend to be blue with $(J-K)_b^c \sim 0.9$, comparable to the disk color. This bulge color in Seyfert 2s is significantly (95% one-tailed) bluer than $(J-K)_b^c$ in normal bulges.

Bulge and disk $J-K$ colors plotted versus $\langle\mu^c(K)\rangle_e$ and $M(K)$ are shown in Fig. 3. There may be a slight trend for bright bulges to have redder colors, but the anomalous bulge colors $[(J-K)_b^c \gtrsim 1.2]$ do not conform to the trend. The tightness of the disk colors is evident in the right panels of Fig. 3. Neither bulge nor disk colors depend on the component absolute luminosity.

We have compared the fitted bulge and disk colors to the inner and outer disk colors derived in Paper I. The inner disk colors in Paper I were defined from averaging the elliptical profiles from 4 arcsec to 3 kpc, and the outer from 3 kpc to the noise limit of the profile. While the 1D outer colors correlate well with the 2D-fitted disk colors, there is very little connection between the 1D inner colors and those of the 2D-fitted bulge. Given the small bulge r_e in our samples, together with the brightness of the disk, the disk contribution becomes comparable to that of the bulge well within the 3-kpc limit, and thus "contaminates" the inner light. It appears that to properly measure colors of the bulge, especially the relatively compact

TABLE 2
SAMPLE MEDIANS OF STRUCTURAL PARAMETERS

Component (1)	Parameter (2)	Active Seyfert 1 (3)	Active Seyfert 2 (4)	Active SBN (5)	Normal Spirals Sa's (6)	Normal Spirals Sc's (7)
Bulge	n_{best}	2	3	1	3	2
	ϵ_b	0.089	0.018	0.231	0.238	0.015
	r_e (kpc)	0.98	0.59	0.75	1.12	1.88
	$\mu_e^c(K)$	16.2	15.7	16.3	16.7	18.1
	$(J-K)_b^c$	1.04	0.87	0.99	1.07	···
	$(H-K)_b^c$	0.17	0.18	0.21	···	0.25
	$M_b(K)$	−23.5	−22.6	−22.7	−23.0	−22.7
Disk	r_d (kpc)	2.5	2.1	2.8	3.2	7.7
	$\mu_d^c(K)$	16.6	16.7	17.3	17.2	18.3
	$(J-K)_d^c$	0.94	0.93	0.87	0.90	···
	$(H-K)_d^c$	0.21	0.20	0.25	···	0.18
	$M_d(K)$	−24.2	−23.6	−23.3	−23.5	−23.8

ones observed in Seyferts and SBNs (and Sa's), the effects of the disk and nucleus need to be removed, a task that is best accomplished with (2D) decomposition.

5. Statistical Comparisons

The Kolmogorov-Smirnov (K-S) test evaluates the probability that two observed cumulative distributions have been drawn from the same parent population. We have applied the K-S test to each pair of samples for each parameter, on the basis of the distributions shown in Fig. 2. The results are illustrated schematically in Fig. 4. As mentioned in the caption, we distinguish between low significance level (between 90% and 95% shown in lower case), moderate (between 95 and 99% in upper case), and high (> 99% in bold face). Although only those differences at 95% or greater should be considered significant, certain trends emerge when the lower-probability differences are taken into account.

5.1. Comparative Summary

Bulges of Seyfert, SBN, and normal spirals are similar to one another in most photometric properties. The most salient difference is between the bulges of normal early- and late-type spirals, as Sa bulges on average are $> 1\,K$-mag arcsec^{-2} brighter than those in Sc's. This result confirms the work of de Jong (1996), who found that early-type bulges are characterized by brighter μ_e, independently of the type of bulge parameterization (n_{best}).

Disk properties differ substantially among the different spiral and active types. Fig. 4 shows that the Sc disks differ significantly from those of early-type and active spirals: they are measurably more tenuous and extended than their early-type counterparts. Indeed, there appears to be a progression from large, tenuous late-type spiral disks ($r_d > 5$ kpc and $\mu_d^c(K) \sim 18$), to brighter and more compact early-types ($r_d \sim 3$ kpc and $\mu_d^c(K) \sim 17$). While part of this behavior may result from selection effects[3], MGH1 also found that early-type spiral disks are more than 1 mag arcsec^{-2} brighter than late-type disks (Giovanardi & Hunt 1988), similar to the trend of early- and late-type bulges.

The K-S tests also show that Seyfert disks are *significantly brighter* even than Sa disks. Seyfert disks are also compact, but not significantly more so than the Sa's, and like early-type disks, they are signif-

[3]The Sc's are taken from a minimum-diameter sample which is expected to be less biased against low-SB objects than are magnitude-limited samples (McGaugh et al. 1995).

icantly more compact than those in late-type spirals. Although the Seyferts, SBNs, and Sa's are selected from magnitude-limited samples which tend to be biased against low surface-brightness objects (McGaugh et al. 1995), they are also "maximum-diameter" selected (the Sa's explicitly so, and the Seyferts and SBNs indirectly so because of the redshift constraint). Furthermore, as mentioned in § 2, the median luminosities and spreads of the different samples are comparable. The similarity of the selection criteria and luminosities among the Seyferts, SBNs, and Sa's would therefore suggest that any bias is not acting "differentially" to affect our results.

5.2. Correlations of Surface Brightness and Scale Length

We investigate here whether bulge and disk parameters for Seyferts and SBN's obey relations similar to those in normal spirals. Correlations between surface brightness and scale length in elliptical galaxies and of bulges and disks in spiral galaxies have been known for some time (Kormendy 1977; Hoessel & Schneider 1985; Djorgovski & Davis 1987; Kent 1985; Kodaira, Watanabe, & Okamura 1986). These two parameters, in fact, constitute an almost face-on view of the "fundamental plane" (FP) for bulges and ellipticals (e.g., Kormendy & Djorgovski 1989, and references therein).

Figure 5 shows plots of bulge and disk SB against respective effective scale lengths[4]. The Seyfert and SBN parameters are shown in the upper panels, and the normal galaxies in the lower panels. Also shown in the lower left panel are bulges taken from Bender, Burstein, & Faber (1992) and Andredakis, Peletier, & Balcells (1995) converted to the K band according to the prescription given by Andredakis et al. The dotted lines in the left panels show the best-fit line to our normal Sa and Sc bulges[5]. The best-fit slope of 2.90 corresponds to $r_e \propto I_e^{-0.86}$, very similar to what is found by Bender et al. (1992) and earlier work (e.g., Kormendy & Djorgovski 1989). Moreover, the intercept relative to the B-band conversion gives a mean $B-K$ color of 3.8, which is a rather normal color for these systems. The upper left panel in Fig. 5 shows that the Seyfert and SBN bulges follow very closely the trend defined by normal spiral bulges and ellipticals.

The situation changes for the disks. We have fit our normal Sa and Sc disks in the same way as for the bulges[6], and find a best-fit slope of 2.94, similar to the bulge value, and corresponding to $r_e \propto I_e^{-0.85}$, identical to that found for ellipticals. This regression is shown, with the normalization appropriate for normal disks, as the lower dotted line in the right panels of Fig. 5; the upper dotted line shows the analogous trend for the bulges, repeated from the left panels. The figure shows that, for a given disk r_e, Seyfert disks have a mean SB $0.9\,K$ mag arcsec^{-2} *brighter* than those in even early-type spirals, comparable to the typical surface brightnesses of the bulge. This appears to be another confirmation of the abnormally bright surface brightness of Seyfert disks.

5.3. Mass-to-Light Ratios

To complete our discussion of the properties of Seyfert host galaxy components, we have collected kinematic data from the literature in the form of central velocity dispersions (Nelson & Whittle 1995; Prugniel & Simien 1996) and neutral hydrogen velocity widths (RC3). These data have been used to derive global mass-to-light (M/L) ratios for the galaxies, and relative M/L ratios for their bulges. Global galaxy M/Ls rely on an effective radius r_{eff} for the galaxy as a whole, obtained by analytically integrating the bulge+disk model. Hydrogen velocity widths have been corrected for inclination (using fitted values) and turbulence. As in Burstein et al. (1997), we have used the expression for κ_3 to calculate relative bulge M/Ls ($\kappa_3 \equiv (\log \sigma_c^2 - \log I_e - \log r_e)/\sqrt{3}$), and r_{eff} to calculate global masses.

It turns out that effective K-band M/L ratios of Seyfert galaxies tend to be slightly smaller than those of normal early-type spirals (median Seyfert $M/L = 0.7$, median Sa $= 0.9$ in solar units). If the actively star-forming Sa's are eliminated from the median[7] (see MGH1), then the Seyfert M/L ratios result almost a factor of two smaller (median true Sa

[4]The disk exponential folding length r_d has been converted to the half-light radius, so that the bulge and disk plots have the same units.

[5]The slope is calculated as the ordinary least-squares (OLS) bisector given by Isobe et al. (1990), and the intercept is defined by forcing the regression to pass through the barycenter of the data points.

[6]The low-luminosity systems in the Sc sample, UGC 628 and UGC 12845, have been omitted from the fit. Given that in dwarf galaxies the trends of scale length r and μ are contrary to those in luminous systems where r increases with fading μ (Binggeli & Cameron 1991), this should be legitimate.

[7]Hereafter, this subset of Sa's will be denoted as "true Sa's".

= 1.2); the difference in the sample means (0.8 for Sy's vs. 1.5 for true Sa's) is significant at the 96% (one-tailed) level. These M/L ratios are plotted in the upper panels of Fig. 7.

We would argue that the lower M/L ratio of Seyferts is due to their *disks*. While Nelson & Whittle (1996) attribute an offset in Seyfert bulge luminosity versus velocity dispersion regressions (e.g., Faber-Jackson) to reduced *bulge* M/L, a Faber-Jackson plot for the bulges in our samples reveals no significant offset between Seyferts and Sa's. A possible explanation of the discrepancy lies in their determination of bulge luminosity, which relies on mean bulge-to-disk ratios as a function of morphological type (e.g., Simien & de Vaucouleurs 1986). For the Seyferts (especially Type 1) in our sample such corrections, on average, *overestimate* the bulge by 0.6 mag; instead, the normal early-type bulges are well determined with the standard correction, having a mean error of 0.1 mag. For a given morphological type, therefore, B/D ratios for Seyferts appear to be somewhat smaller than those of normal spirals. Indeed, the Sy 1's, similar to the Sa's in almost every way, have significantly more luminous disks (see Fig. 4), an effect which probably results from their high surface brightnesses as shown in the upper right panels of Figs. 3 and 5. The mean difference of 0.6 mag that we find between Seyferts and normal early-type spirals is perhaps fortuitously similar to Nelson & Whittle's mean offset of 0.7 mag, but may be an explanation for the disagreement.

We have also placed Seyferts, SBNs, and Sa's in the fundamental plane according to the formalism of Burstein et al. (1997, see also Bender et al. 1992). Figure 6 shows various projections of the FP together with the B-band relations defining the FP in the κ_1/κ_3 projection (shown as a solid line), and the "zone of exclusion" in κ_1/κ_2. As before, our data have been converted from K to B according to Andredakis et al. (1995). In these projections of the FP at a given mass, the M/Ls of Seyfert *bulges* (upper left panel) are very similar to those in normal spiral bulges. In contrast, our K-band data for global M/Ls (upper right panel) do not strictly conform to the FP as defined in B by Burstein et al. (1997). However, because of our small sample sizes (further reduced by the available kinematic data), we have not determined a slope, but rather fixed it to the canonical one, and for each sample adjusted the intercept ("offset") in a least-squares sense. The offsets for Sy's (shown as dotted line) and true Sa's (dashed line) differ significantly (99.9% –one-tailed– level), again with Sy's having global M/Ls almost a factor of two lower. This result, though, is not independent of the smaller Seyfert M/L ratio previously discussed, since it depends on the same input quantities. What we have shown here is that while true Sa's conform to the FP, Seyferts do not; they tend to have, in the mean, lower global M/Ls.

We therefore find no evidence for a systematically lower M/L ratio in Seyfert bulges, relative to normal early-type spirals, but rather for smaller *global* M/L ratios in Seyfert galaxies. In the absence of spatially-resolved kinematic data, it is not straightforward to determine absolute M/L ratios of the bulge and disk, but indirect arguments seem to suggest that the Seyfert disk, not the bulge, is the galaxy component with an anomalously low M/L ratio. This point will be discussed further in the next section.

5.4. Neutral Hydrogen Content

We have calculated two quantities, both evaluated with r_{eff}, to measure the neutral hydrogen content in our samples: the mean HI surface density σ_{HI}, and the HI mass fraction M_{HI}/M_{eff}. Seyfert, SBN, and Sc median σ_{HI} are typical of spiral types Sb or later (Roberts & Haynes 1994), while Sa's show median σ_{HI} three or four times lower, consistent with normal early-type spirals (Eder et al. 1991). In terms of neutral hydrogen mass fraction, SBN's have the highest median M_{HI}/M_{eff} of all the samples ($\sim$ 40-50%), with Seyferts following at 18% (14% for Type 1's, 20% Type 2's). Sa's at 4% are consistent with normal early-type spirals (Roberts & Haynes 1994; Broeils & Rhee 1997). On the basis of both criteria, therefore, we conclude that Seyferts, although structurally very similar to Sa's, are much richer in neutral gas. Indeed, even normal very late-type spirals are observed to have $M_{HI}/M_{\mathit{eff}} \lesssim 10$–$12\,\%$ (Roberts & Haynes 1994), so that the Seyferts, and especially SBNs, appear to have abnormally high neutral gas fractions, independently of their morphological type. If the molecular gas were taken into account, the work of Maiolino et al. (1997) shows that we could even be underestimating the total gas content in these systems by a factor of two or more.

We also find the HI mass fraction M_{HI}/M_{eff} in Seyferts and SBNs to be anticorrelated with effective M/L ratio. This anticorrelation is shown in the upper middle panel of Fig. 7 where lower M/L is seen together with higher M_{HI}/M_{eff}, but the trend

is amplified by the use of M_{eff} in both plotted variables. To assess the impact of this on the correlation, we have performed Monte Carlo experiments that reproduce the statistical characteristics of the combined Sy+SBN sample (in terms of mean and spread in L_K, M_{eff}, M_{HI}, and the correlations between them). Results show (via the Fisher z test, see Bulmer 1967) that the anticorrelation between M_{HI}/M_{eff} and M/L is significant at the 96% (two-tailed) level (2σ), independently of underlying correlations and those induced by correlated measurement uncertainties. The behavior of the Sa's, on the other hand, is well-reproduced by the Monte Carlo experiments, appearing to depend solely upon the underlying biases.

The dependence of gas content on M/L is also shown in the upper right panel of Fig. 7, where M/L is plotted against σ_{HI}. The HI surface brightness is independent of distance, and the correlation should be more free of systematic effects than M_{HI}/M_{eff} vs. M/L; σ_{HI} and M/L are again significantly correlated in Seyferts and SBNs at the 2σ level. Nevertheless, true HI surface brightness is only very crudely estimated by the values reported here, and we would argue that the more physically significant variable is M_{HI}/M_{eff}. Even for anomalously high gas mass fractions, spatially resolved HI maps are needed to determine if Seyferts and SBNs really do have, for a given morphology, higher-than-average HI surface density.

We also find in Seyferts and SBNs a correlation ($\gtrsim$ 95% two-tailed) between $\mu_d(K)$ and HI mass fraction, in the sense that fainter $\mu_d(K)$ implies higher M_{HI}/M_{eff}. This trend, shown in the lower left panel of Fig. 7, is displaced from normal spirals, and the clear segregation between active and normal spirals is indicated by the diagonal dotted line. Since HI tends to be associated with the stellar disk, these are yet more indications that the low M/L ratios we and others find in Seyfert galaxies are a property of the disk, and not of the bulge.

6. Summary, Discussion, and Speculation

We summarize here what has emerged from our investigation, and then speculate about what the results might imply.

- In normal spirals, we confirm the trends found in earlier studies of bulge and disk parameters with morphological type: early-type spiral bulges are brighter (μ_e) than late-types (de Jong 1996), and Sa disks are more compact (r_d) and bright (μ_d) than those in Sc's (GMH1).

- Seyfert and SBN bulges resemble normal bulges in structure and color, with $(J-K)_b^c$ about 0.1 mag redder than disk $(J-K)_d^c$, except that: *i*) Sy 2 bulges tend to be rounder than those in Sy 1's and normal spirals; *ii*) Sy 2 bulges have $(J-K)_b^c \sim (J-K)_d^c$ (see also Paper I).

- Seyfert disks (especially Type 1), but not those of SBNs, are significantly brighter than early-type disks, which are, as mentioned above, brighter than those of Sc's. Evidence of this result is seen in the K-S comparision (Fig. 4) and in the trends of disk SB and radius (Fig. 5). Seyfert disks are also compact, but not significantly more so than those in early-type spirals. We also find some suggestion (Fig. 4) for, at a given morphological type, higher disk *luminosity* in Sy 1's (hence reduced bulge-to-disk ratios) which we attribute to their higher disk surface brightness.

- Seyferts, and especially SBNs, are very rich in neutral gas: while neutral gas fractions M_{HI}/M_{eff} for normal spirals are observed to be $\lesssim$ 10%, Seyferts have M_{HI}/M_{eff} of around 18%, and SBNs $\gtrsim$ 40%. This trend is illustrated in Fig. 7, where the different properties of normal and active spirals are evident.

- We find strong, albeit indirect, evidence for lower M/L ratios in Seyfert and SBN *disks*, but for normal M/Ls in their bulges. Such evidence includes normal (i.e., without offset) Faber-Jackson plots for Seyfert bulges; an offset in the FP, not for the bulges, but rather towards lower *global* M/L ratios (Fig. 6); and anticorrelations of M/L with what are usually thought to be a disk quantities, namely HI mass fraction and surface density (Fig. 7).

First, we find Seyfert disks to be anomalously bright, relatively compact, and, for their mass, abnormally rich in HI. Evolutionary simulations of disk galaxies suggest that such disks might be the product of mass transport from the outer regions to the center, and the ensuing episode(s) of star formation. Models of galaxies with a stellar bulge, disk, and a gas component show a significant central buildup of *stars and gas* after 2 Gyr (Junqueira & Combes 1996). In

the Junqueira & Combes models, the evolved stellar (and gaseous) distributions show progressively brighter central surface brightnesses and smaller effective radii, similar to those we observe in Seyfert galaxies. The weak trend (Fig. 7) we find for dimmer $\mu_d(K)$ at higher M_{HI}/M_{eff} in Seyferts and SBNs (and perhaps in normal spirals, see McGaugh & de Blok 1997) may also support this scenario: the more gas already converted into stars, the lower the gas mass fraction, and the brighter the disk.

Second, such secular buildup and central concentration of stars and gas occurs in the simulations *even in the absence of a bar*. The high neutral gas mass fraction in Seyferts (and SBNs) may be an explanation for the discordant findings of incidence of bars and interactions in Seyfert galaxies (see Introduction and references therein). The simulations of Junqueira & Combes (1996) correspond to a gas fraction of 10%, but, as noted by them, when gas mass fractions exceed roughly 10%, the gas can damp bar instabilities, instead of exciting them (Shlosman & Noguchi 1993). The abnormally abundant neutral gas in Seyferts may therefore prevent the formation of bars in Seyfert disks; the gas gets funnelled inward anyway because of dynamical friction (Shlosman & Noguchi 1993) or spiral wave instabilities (Junqueira & Combes 1996; Zhang 1996).

Third, the anticorrelation between M/L and M_{HI}/M_{eff} suggests that SBN and some Seyfert disks have undergone or are undergoing more star formation than normal spirals. For a given age, M/L ratios measured at wavelengths longward of about 1 μm decrease with metallicity (Worthey 1994), and, at a given metallicity, increase with age. According to the Worthey models, the expected range due to age is 0.5 dex for ages $\gtrsim 2$ Gyr, and in metallicity less than half that. Because the M/Ls observed here anticorrelate with neutral hydrogen mass fraction, and because their variation has an amplitude (~ 2 dex) that exceeds by far the spread predicted by the Worthey models, we claim that the M/L ratios indicate a very young age, not extreme metallicity. If this is true, the low M/L ratios and high M_{HI}/M_{eff} imply that the SBNs and some Seyferts are actively forming stars, and their stellar populations are relatively young (< 2 Gyr). Turning again to Fig. 7, we add that among Seyfert and SBNs, and perhaps separately among normal spirals, the more gas already converted into stars, the higher the M/L, and the older the mean age of the stellar population.

As to differences in star formation histories between Seyfert 1s and 2s, we are not able, because of our small samples, to make conclusive statements. Although the statistics are very poor, Type 2 Seyferts may have a higher HI mass fraction than Type 1s, suggesting that star formation may have occurred more recently in Seyfert 2s (Paper I; Oliva et al. 1995). The blue disk-like color and roundness of Seyfert 2 bulges are probably relevant here. Blue $J-K$ bulge colors should indicate younger age or lower metallicity or both, although we have very little color leverage to disentangle the combined effects of age and metal abundance. We can only point out that Seyfert 2 bulges are more similar to normal and active spiral *disks*, than to normal bulges, or to the bulges of Type 1 Seyferts and SBNs.

Finally, we address the question of an evolutionary link between Seyfert, SBN, and normal bulges and disks. Normal early-type spiral bulges and disks are brighter and more compact than those of late types. Since we argued above that bright, compact disks could result from inward mass transport in Seyferts, we could speculate in a similar vein that normal early-type disks have evolved, over time, from late-types. The central depression in neutral hydrogen commonly observed in early-type spirals (e.g., van Driel & van Woerden 1991) would result naturally from such a scenario, since presumably the gas would be blown out (e.g., Israel & van Driel 1990) or consumed (van Driel & van Woerden 1991) by violent star formation in the central regions. Disk evolution is also compatible with recent work that suggests that the rate of galaxy evolution depends on disk surface density. Gas consumption is delayed in low-surface-brightness systems, and brighter disks are more evolved, having undergone more episodes of star formation in the past (McGaugh & de Blok 1997).

We speculate further that Seyferts may be extreme cases of high (initial and present) HI mass fraction coupled with high-density, evolved disks at the current epoch. Because of their high gas content, Seyfert disks have continued to undergo episodes of star formation up to now, consuming the gas, but not yet exhausting it. Early-type spirals would be those which did not have sufficient gas initally to create either a bright Seyfert-like disk or an active nucleus, and SBNs would not yet have had enough time to build up either one, but may do so in the future given the large reservoir of gas available. The rate of bulge/disk/active nucleus evolution in spirals would be determined by

the gas fraction, the efficiency and time scale of the inward mass transport, and by the rate and efficiency of star formation.

We would like to thank Edvige Corbelli, Daniele Galli, and Francesco Palla for interesting discussions; Carlo Giovanardi for insightful comments; and an anonymous referee for probing questions that resulted in a better paper. This research was partially funded by ASI Grant ARS-96-66.

REFERENCES

Andredakis, Y.C., Peletier, R.F., & Balcells, M. 1995, MNRAS, 275, 874

Arsenault, R. 1989, A&A, 217, 66

Balzano, V.A. 1983, ApJ, 268, 602

Barnes, J.E. & Hernquist, L. E. 1991, ApJ, 370, L65

Bender, R., Burstein, D., & Faber, S.M. 1992, ApJ, 399, 462

Binggeli, B., & Cameron, L.M. 1991, A&A, 252, 27

Broeils, A.H., & Rhee, M.-H. 1997, A&A, 324, 877

Bulmer, M.G. 1967, "Principles of Statistics", Dover Publications, Inc., New York

Burstein, D. 1979, ApJ, 234, 435

Burstein, D., Bender, R., Faber, S.M., & Nolthenius, R. 1997, AJ, 114, 1365

Bushouse, H. 1987, ApJ, 320, 49

Byun, Y.I., & Freeman, K.C. 1995, ApJ, 448, 563

Carlberg, R.G. 1986, in Nearly Normal Galaxies, ed. S.M. Faber (New York: Springer), 129

Combes, F., & Elmegreen, B.G. 1993, A&A, 271, 391

Dahari, O. 1985, AJ, 90, 1772

Danese, L., Zitelli, V., Granato, G.L., Wade, R., De Zotti, G., & Mandolesi, N. 1992, ApJ, 399, 38

de Jong, R.S. & van der Kruit, P.C. 1994, A&ASS, 106, 451

de Jong, R.S. 1995, Ph.D. Thesis, University of Groningen

de Jong, R.S. 1996, A&A, 313, 45

de Vaucouleurs, G., de Vaucouleurs, A., Corwin, H. G., Buta, R., Paturel, G., & Fouqué, P. 1991, Third Reference Catalogue of Bright Galaxies (Springer, New York) (RC3)

Djorgovski, S., & Davis, M. 1987, ApJ, 313, 59

Eder, J., Giovanelli, R., & Haynes, M.P. 1991, AJ, 102, 572

Elmegreen, B.G., & Elmegreen, D.M. 1985, ApJ, 288, 438

Fuentes-Williams, T., & Stocke, J. 1988, AJ, 96, 1235

Giovanardi, C. & Hunt, L.K. 1988, AJ, 95, 408

Heller, C.H. & Shlosman, I. 1994, ApJ, 424, 84

Hernquist, L. 1989, Nature, 340, 687

Ho, L.C., Filippenko, A.V., & Sargent, W.L.W. 1997, ApJ, 487, 591

Hoessel, J.G., & Schneider, D.P. 1985, AJ, 90, 1648

Huchra, J. & Burg, R. 1992, ApJ, 393, 90

Hunt, L.K., Malkan, M.A., Salvati, M., Mandolesi, N., Palazzi, E., & Wade, R. 1997, ApJS, 108, 229 (Paper I)

Isobe, T., Feigelson, E.D., Akritas, M.G., & Babu, G.J. 1990, ApJ, 364, 104

Israel, F.P., & van Driel, W. 1990, A&A, 236, 323

Junqueira, S., & Combes, F. 1996, A&A, 290, 785

Keel, W.C. 1996, AJ, 111, 696

Keel, W.C., Kennicutt, Jr., R.C., van der Hulst, J.K., & Hummel, E. 1985, AJ, 90, 708

Kent, S.M. 1985, ApJS, 59, 115

Kodaira, K., Watanabe, M., & Okamura, S. 1986, ApJS, 62, 703

Kormendy, J. 1977, ApJ, 218, 333

Kormendy, J. & Djorgovsky, S. 1989, ARA&A, 27, 235

Kormendy, J., & Richstone, D. 1995, ARA&A, 33, 581

Kotilainen, J.K., Ward, M.J., Boisson, C., DePoy, D.L., & Smith, M.G., 1992, MNRAS, 256, 149

MacKenty, J.W. 1990, ApJS, 72, 231

Maiolino, R., Ruiz, M., Rieke, G.H., & Papadopoulos, P. 1997, ApJ, 485, 552

Malkan, M.A., Gorjian, V., & Tam, R. 1998, ApJS, July, 1998

Mazzarella, J.M. & Balzano, V. 1986, ApJS, 62, 751

McLeod, K.K. & Rieke, G.H. 1995, ApJ, 441, 96

McGaugh, S.S., & de Blok, W.J.G. 1997, ApJ, 481, 689

McGaugh, S.S., Bothun, G.D., & Schombert, J.M. 1995, AJ, 110, 573

Mihalas, D., Binney, J., 1981, Galactic Astronomy, Freeman (San Francisco)

Moles, M., Márquez, I., & Pérez 1995, ApJ, 438, 604

Moriondo, G., Giovanardi, C., & Hunt, L.K. 1998a, A&AS, 130, 81 (MGH1)

Moriondo, G., Giovanardi, C., & Hunt, L.K. 1998b, A&A, in press (MGH2)

Mulchaey, J.S., & Regan, M.W. 1997, ApJ, 482, L135

Nelson, C.H., & Whittle, M. 1995, ApJS, 99, 67

Nelson, C.H., & Whittle, M. 1996, ApJ, 465, 96

Norman, C. 1987, in Star Formation in Galaxies, ed. G. Neugebauer & N. Scoville (NASA Conf. Pub)., CP-2466, 395

Oliva, E., Origlia, L., Kotilainen, J.K., & Moorwood, A.F.M. 1995, A&A, 301, 550

Osterbrock, D.E., & Pogge, R.W. 1991, ApJ, 323, 108

Prugniel, P., & Simien, F. 1996, A&A, 309, 749

Rafanelli, P., Violato, M., & Baruffolo, A. 1995, AJ, 109, 1546

Roberts, M.S., & Haynes, M.P. 1994, ARA&A, 32, 115

Rubin, V.C., Burstein, D., Ford, W.K., & Thonnard, N. 1985, ApJ, 289, 81

Sandage, A., & Tammann, G. 1981, *A Revised Shapley-Ames Catalog of Bright Galaxies* (Washington D.C.: Carnegie Institution of Washington)

Sèrsic, J.-L. 1968, Atlas de Galaxias Australes (Cordoba: Observatorio Astronomico)

Shlosman, I., Begelman, M., & Frank, J. 1989, Nature, 338, 45

Shlosman, I., & Noguchi, M. 1993, ApJ, 414, 474

Simien, F. & de Vaucouleurs, G. 1986, ApJ, 302, 564

Sparks, W.B. 1988, AJ, 95, 1569

Terlevich, R., Tenorio-Tagle, G., Franco, J., & Melnick, J. 1992, MNRAS, 255, 713

van Driel, W., & van Woerden, H. 1991, A&A, 243, 71

Worthey, G. 1994, ApJS, 95, 107

Yee, H.K.C. 1983, ApJ, 272, 473

Zhang, X. 1996, ApJ, 457, 125

Fig. 1.— J-band major-axis cuts together with the best-fit decomposition. The observed and fit $J-K$, $J-H$, and $H-K$ color profiles are also shown; these are merely the difference of the major-axis cuts in the various filters. The major-axis cuts are shown as crosses, and elliptically-extracted profiles (see Paper I) are shown as open circles. Error bars indicate the uncertainties used in the 2D decomposition, and may be dominated by asymmetries as described in the text. The top horizontal axis shows galactocentric distance in kpc, assuming the distances given in Table 1, and the bottom galactocentric distance in arcsec. Bulge n_{best} is shown in the upper right corner below the object name. The three components are shown in the upper panel as long dashed lines, and their sum in all panels as short dashed lines. The fits take into account the different seeing widths in the different bands, but the observed profiles have not been rebinned. The profile of Mrk 993, the most highly inclined galaxy in our samples, shows a good example of the difference between elliptically-averaged profiles and the major-axis cut. Not only do the surface brightnesses differ substantially in the central region, but also the colors ($J-K$, $J-H$).

This 2-column preprint was prepared with the AAS LaTeX macros v4.0.

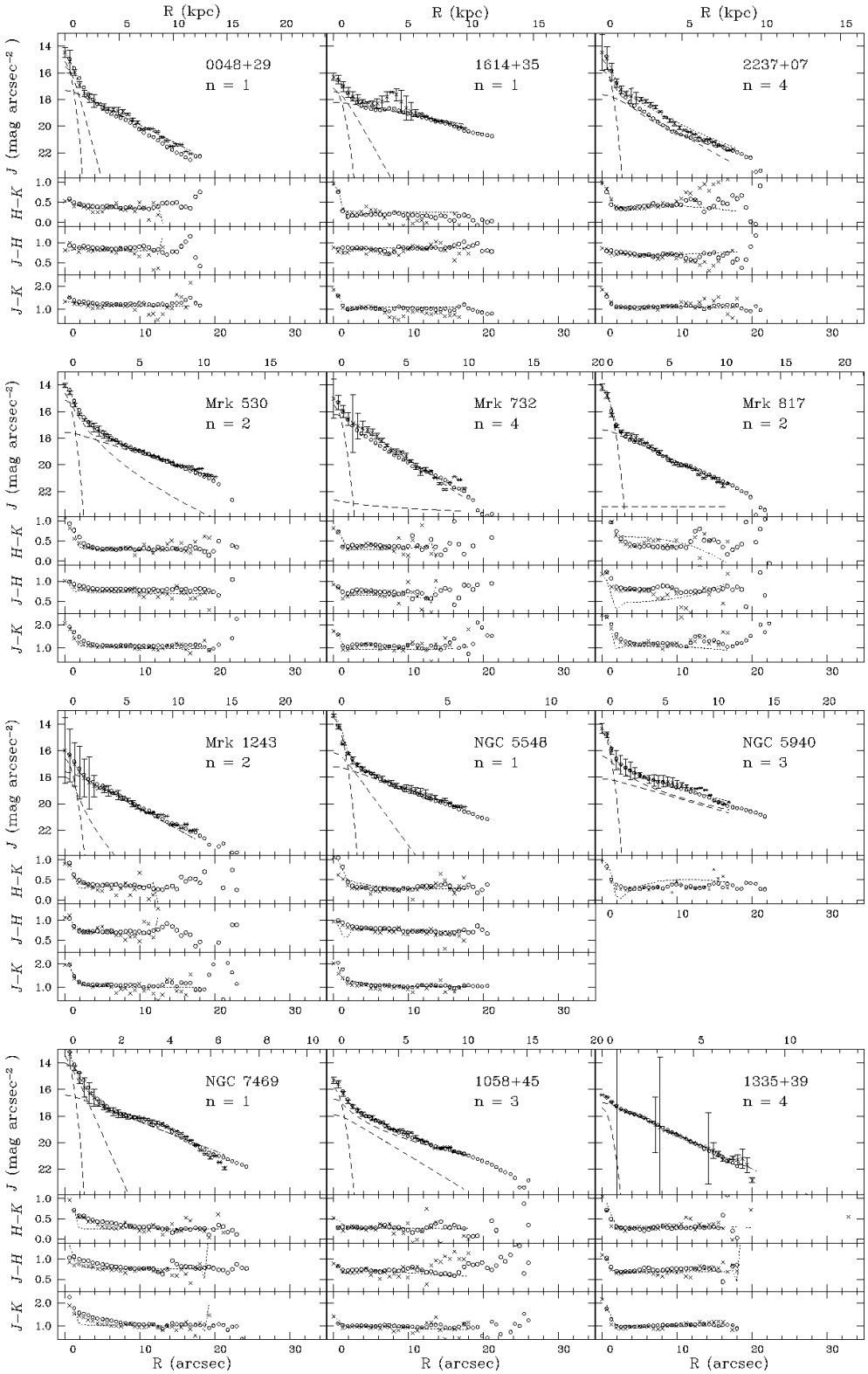
R (kpc)
0048+29
n = 1
1614+35
n = 1
2237+07
n = 4
Mrk 530
n = 2
Mrk 732
n = 4
Mrk 817
n = 2
Mrk 1243
n = 2
NGC 5548
n = 1
NGC 5940
n = 3
NGC 7469
n = 1
1058+45
n = 3
1335+39
n = 4
J (mag arcsec⁻²)
H–K
J–H
J–K
R (arcsec)

Fig. 1a

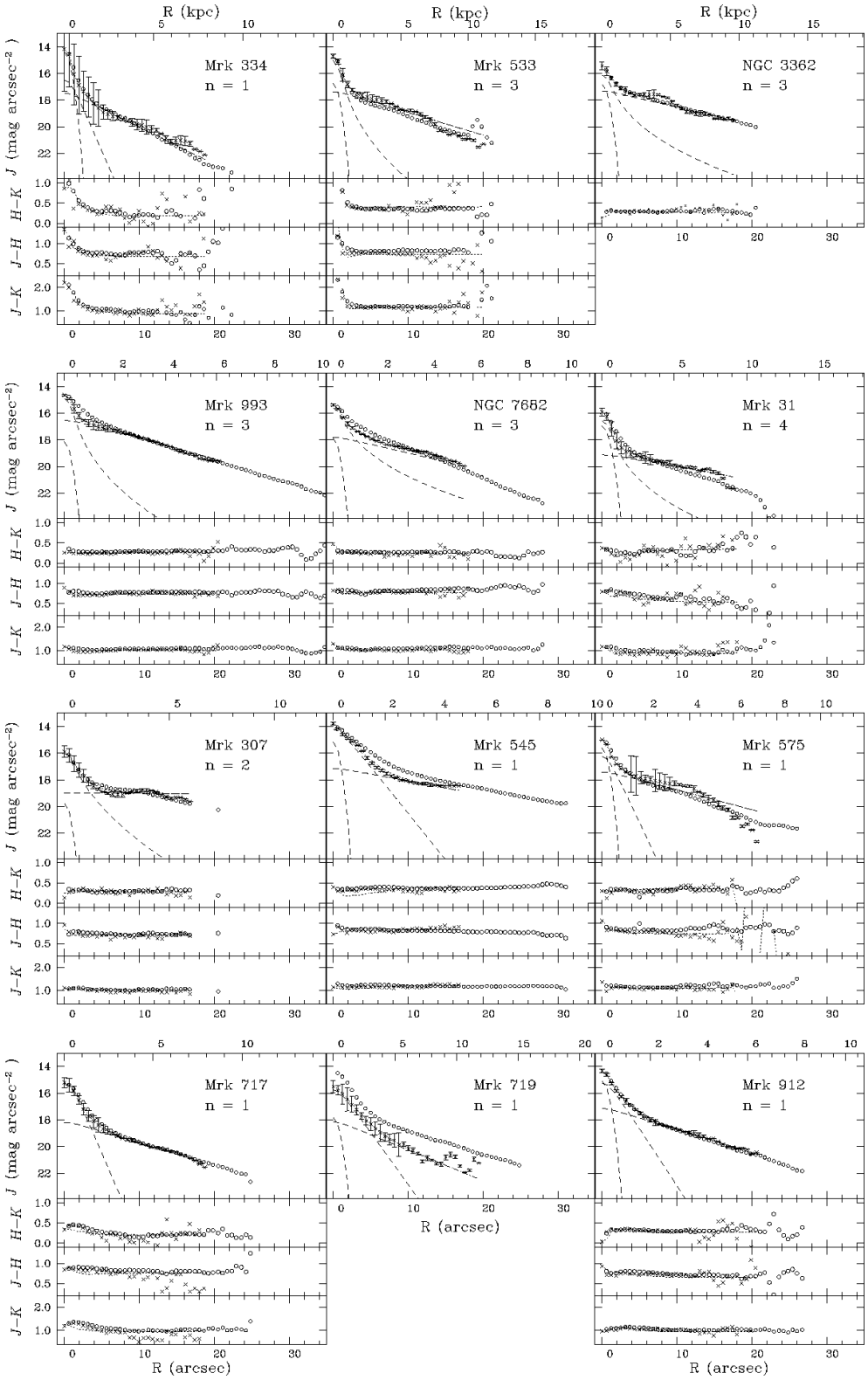
R (kpc)
Mrk 334
n = 1
Mrk 533
n = 3
NGC 3362
n = 3
Mrk 993
n = 3
NGC 7682
n = 3
Mrk 31
n = 4
Mrk 307
n = 2
Mrk 545
n = 1
Mrk 575
n = 1
Mrk 717
n = 1
Mrk 719
n = 1
Mrk 912
n = 1
J (mag arcsec⁻²)
H–K
J–H
J–K
R (arcsec)

Fig. 1b

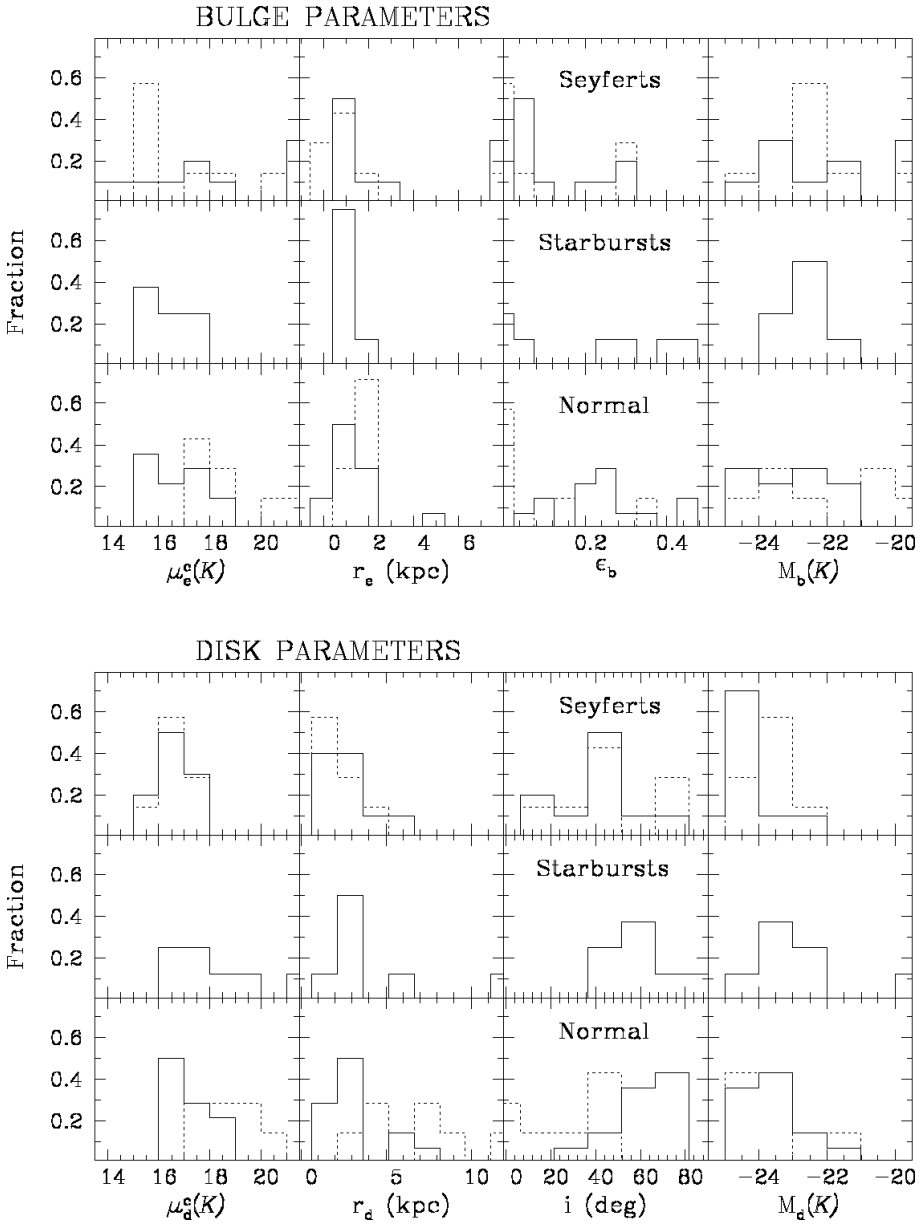

Fig. 2.— Observed distributions of fitted parameters for each component as a function of galaxy activity class. Illustrated for bulge (top panel) and disk (bottom panel) are the K-band surface brightnesses and absolute luminosities, scale lengths, and ellipticities/inclinations. The top panel for each component shows Type 1 Seyferts as solid lines, and Type 2 as short-dashed lines; the middle panel shows SBNs; the bottom panel shows Sa's as solid lines, and Sc's as short-dashed lines.

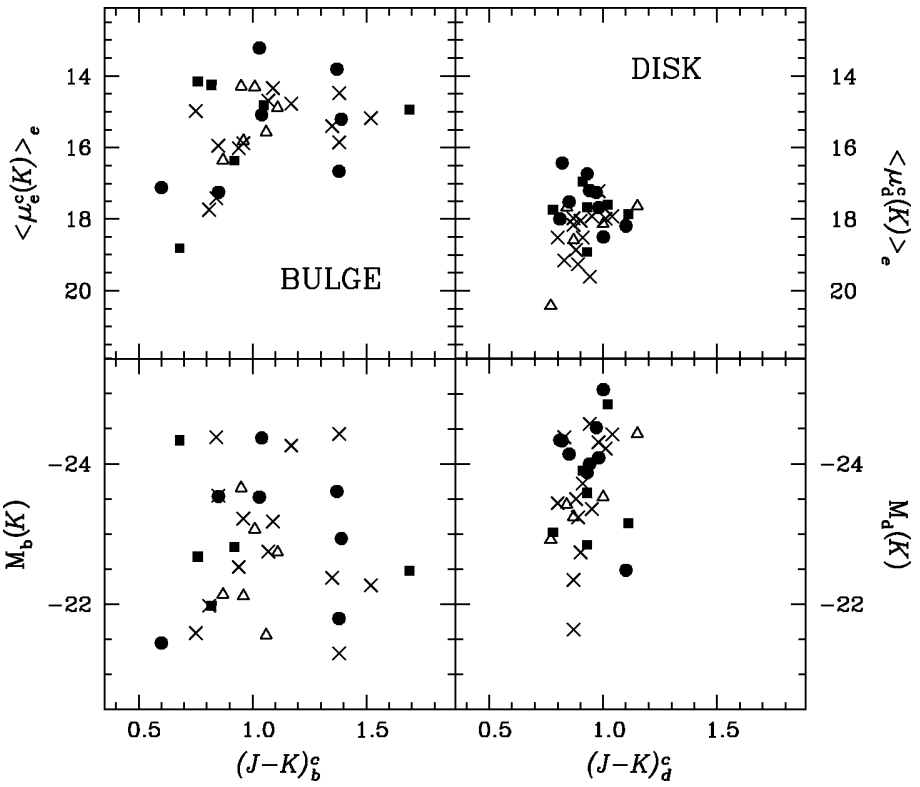

Fig. 3.— Plots of mean surface brightness $< \mu^c(K) >_e$ and luminosity $M(K)$ versus $(J-K)^c$. Bulge parameters are shown in the left panels, and disks on the right. Seyfert 1s are denoted by filled circles, Seyfert 2s by filled squares, SBNs by open triangles, Sa's by $\times$, and Sc's by $+$.

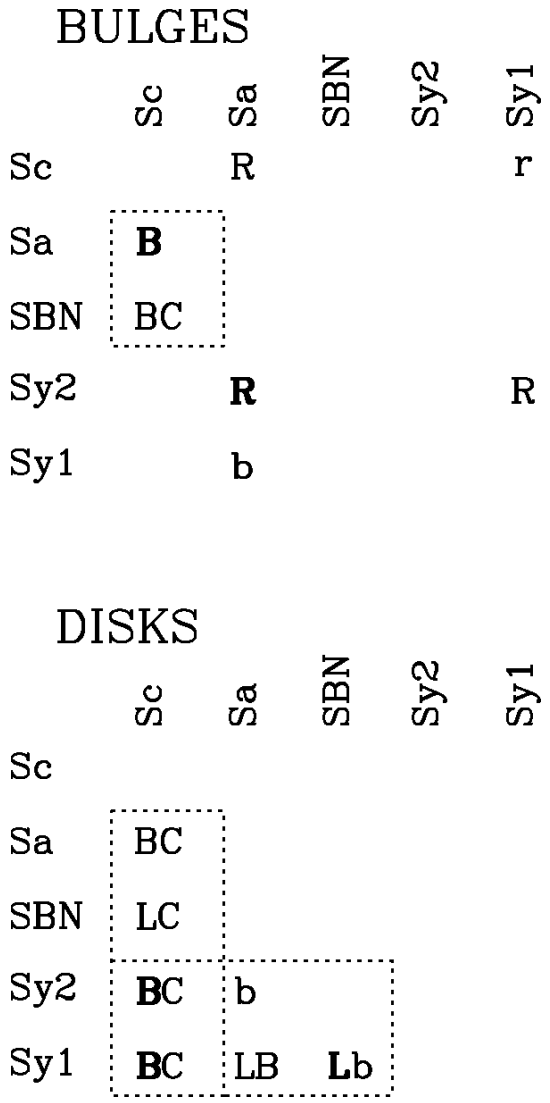

Fig. 4.— A graphic summary of the statistical analysis described in § 5. The upper panel refers to bulge properties, the lower one to disks. The letters indicate the quantity for which a significant difference was found between the two given subsamples: B stands for surface brightness, R for roundness of bulges (i.e. rounder bulges have smaller ϵ_b), C for compactness (i.e. more compact components have smaller physical scale length), and L for luminosity. The sign of the difference (i.e., which sample has the largest value of a given parameter) is from left to above, in the sense that for a given comparison, the sample towards the bottom and left has a smaller value of the parameter than the sample to the top and right. The significance of the difference is given by the size of the letter: lower case means a significance level between 90 and 95%, upper case between 95 and 99%, and bold face greater than 99%. For instance, considering only Sc's and Sa's in the upper panel, we see that Sc bulges are rounder than Sa's at between 90 and 95% confidence level, whereas Sa bulges have higher surface brightnesses than Sc's at more than 99%. Dotted lines are given to better delineate the significant differences between samples.

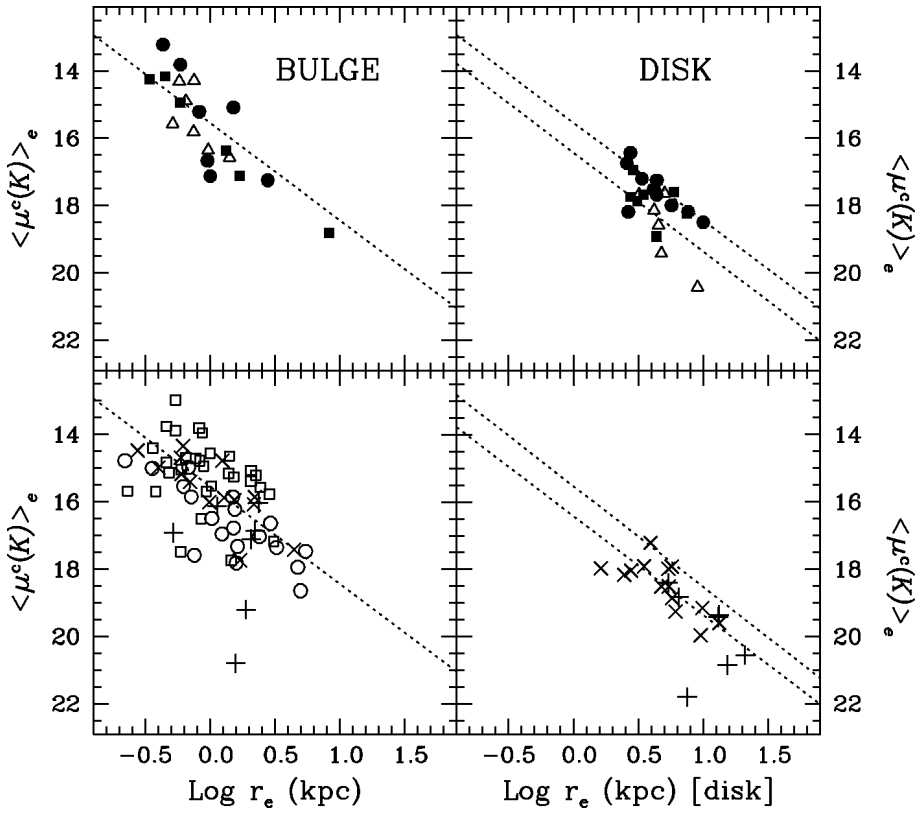

Fig. 5.— Plots of mean surface brightness $< \mu^c(K) >_e$ versus $\log r_e$. Bulge parameters are shown in the left panels, and disks on the right; active spirals are shown in the upper panels, and normal spirals in the lower ones. Disk exponential folding length r_d has been converted to the half-light effective radius r_e, so that bulge and disk plots have the same units. As in Fig. 3, Seyfert 1s are shown as filled circles, Seyfert 2s as filled squares, SBNs as open triangles, Sa's as $\times$, and Sc's as $+$. In the lower left panel, bulges from Bender et al. (1992) and from Andredakis et al. (1995) are shown as open circles and open squares, respectively, converted to K as described in the text. The regressions shown as dotted lines in the left panels are the best fits to our normal bulges as defined in the text. The right panels show the bulge regression as the upper line, and the best fit to the normal disks as the lower line; they have similar slope, but are offset vertically by roughly $0.9\,\mathrm{mag\,arcsec^{-2}}$.

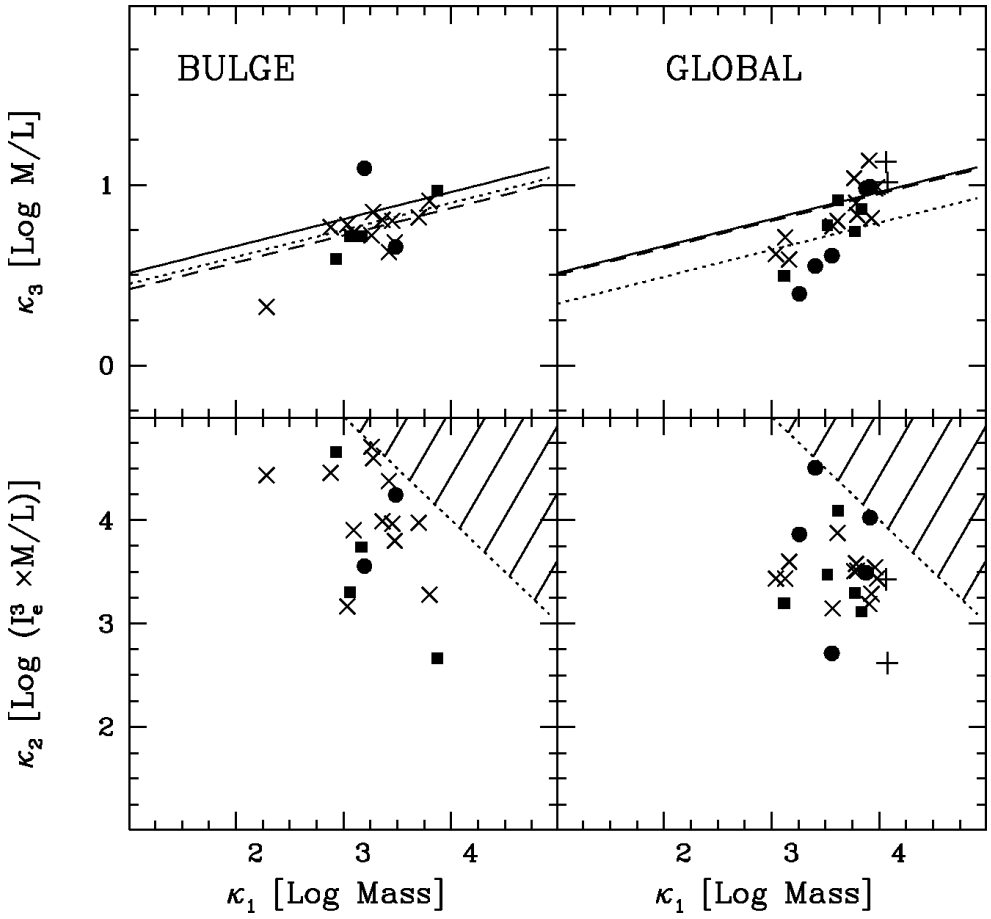

Fig. 6.— κ_1/κ_2 and κ_1/κ_3 projections of the FP as defined in Bender et al. (1992). $\kappa_1 \equiv (\log \sigma_c^2 + \log r_e)/\sqrt{2}$; $\kappa_2 \equiv (\log \sigma_c^2 + 2 \log I_e - \log r_e)/\sqrt{6}$; $\kappa_3 \equiv (\log \sigma_c^2 - \log I_e - \log r_e)/\sqrt{3}$. Bulge parameters are shown in the left panels, with I_e and r_e defined in the K band from our decompositions, and σ_c taken from Nelson & Whittle (1995). Global effective parameters are shown in the right panels, with K-band I_{eff} and r_{eff} derived from the fits as described in the text. HI line widths are taken from RC3, and corrected as described in Burstein et al. (1997). All data have been converted to the B band as described in the text. Symbols are as in Fig. 3. The upper panels, with κ_1/κ_3 shows the solid line defined by: $\kappa_3 = 0.15\,\kappa_1 + 0.36$, and the lower panels with κ_1/κ_2 shows the zone-of-exclusion defined by: $\kappa_1 + \kappa_2 = 8$. Offsets as defined in the text are shown as dashed lines for the Sa's, and as dotted lines for the Sy's. The lower global (effective) M/L for the Seyferts is evident in the upper right panel.

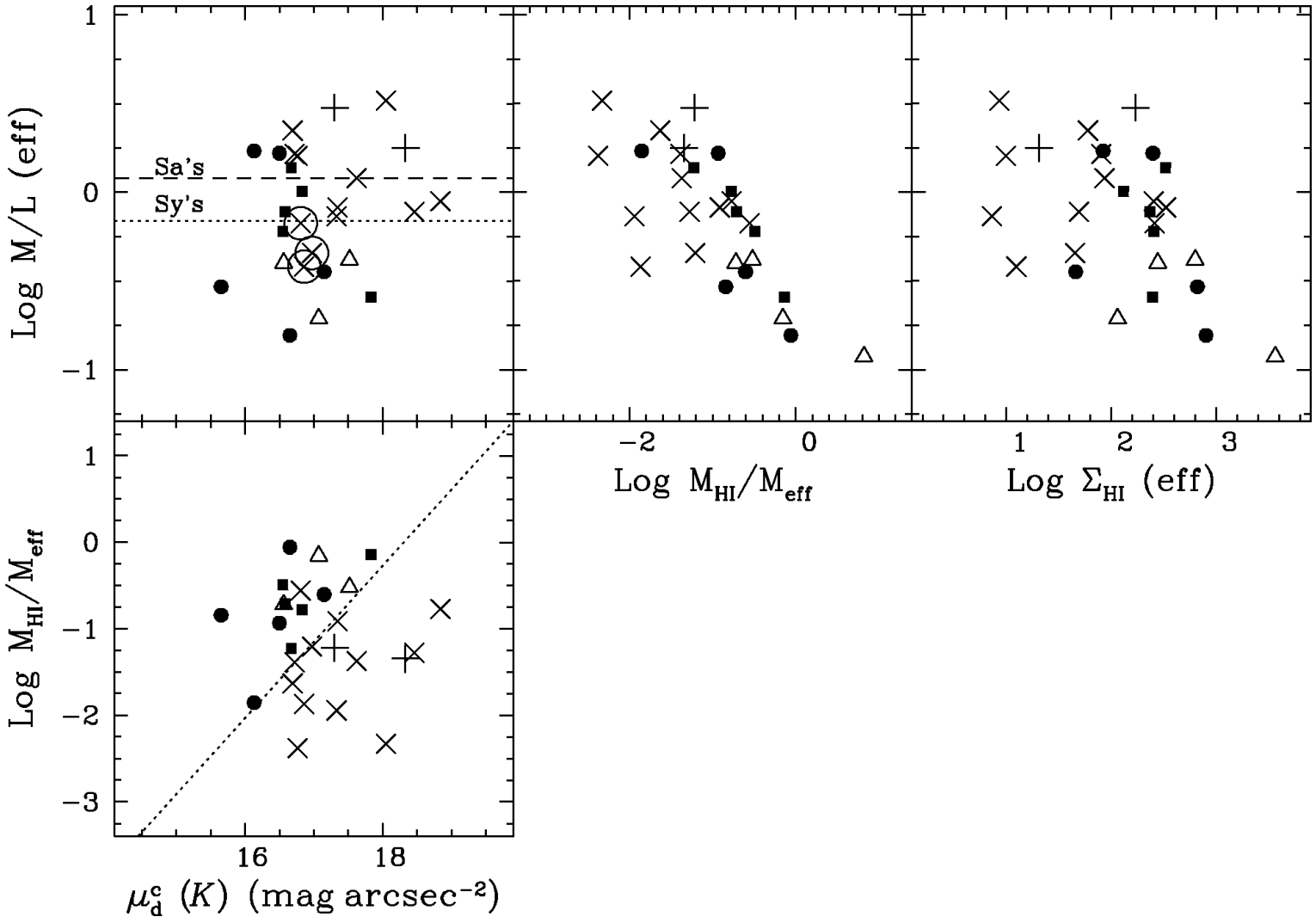

Fig. 7.— Plots of (log) effective M/L versus $\mu_d^c(K)$ (upper left panel); versus (log) neutral hydrogen mass fraction M_{HI}/M_{eff} (upper middle panel); versus (log) neutral hydrogen surface density σ_{HI} (upper right panel); and M_{HI}/M_{eff} versus $\mu_d^c(K)$ (lower panel). M/L ratios are effective (half-light) calculated as described in the text. As in Fig. 3, Seyfert 1s are shown as filled circles, Seyfert 2s as filled squares, SBNs as open triangles, Sa's as $\times$, and Sc's as $+$. The three Sa's in the upper left panel are actively star-forming Sa's (NGC 3593, 4419, 5879), and are marked with circumscribing circles; the median Sa (omitting these) and Seyfert M/L are illustrated with horizontal dotted lines. The dotted line in the lower left panel is not a fit, but rather indicative of the segregation of the "active" and normal spiral classes.

TABLE 1

Structural Parameters

			BULGE							DISK						
Name	Dist.[a]	n_{best}[b]	e_b	r_e[c]	$\mu_e^c(K)$[d]	$(J-K)_e^c$	$(H-K)_e^c$	$M(K)_b$[e]	i[f]	r_d[c]	$\mu_d^c(K)$[d]	$(J-K)_d^c$	$(H-K)_d^c$	$M(K)_d$[e]	$M(K)_g$[e]	χ^2_ν
(1)	(2)	(3)	(4)	(5)	(6)	(7)	(8)	(9)	(10)	(11)	(12)	(13)	(14)	(15)	(16)	(17)
0048+29	143.0	1	0.051	0.85	14.61	1.37	0.32	-23.61	57.9	3.75	16.65	0.98	0.20	-24.09	-24.63	3.1
			(0.04)	(0.09)	(0.27)				(6.7)	(0.14)	(0.09)					
				0.59						2.60						
1614+35	116.1	1	0.304	1.78	17.91	0.60	-0.17	-21.45	47.2	10.54	17.46	1.00	0.15	-25.06	-25.09	6.7
			(0.01)	(0.35)	(0.31)				(13.3)	(0.81)	(0.09)					
				1.00						5.93						
2237+07	97.2	4	0.218	5.89	18.70	0.85	0.02	-23.54	70.0	3.34	17.13	1.10	0.60	-22.49	-23.89	4.2
			(0.04)	(0.61)	(0.23)				(20.2)	(0.28)	(0.21)					
				2.78						1.57						
Mrk 530	115.9	2	0.109	2.68	16.21	1.04	0.21	-24.37	49.0	6.02	16.97	0.81	0.15	-24.34	-25.11	1.7
			(0.01)	(0.26)	(0.13)				(7.7)	(0.28)	(0.14)					
				1.51						3.38						
Mrk 732	119.2	4	...	...	...	...	...	...	47.9	2.83	15.39	0.82	0.17	-24.33	-24.33	3.6
			...	...	...				(8.0)	(0.18)	(0.08)					
				...						1.64						
Mrk 817	130.2	2:	...	...	...	...	...	...	21.9	4.12	16.21	0.97	0.55	-24.52	-24.52	21.3
			...	...	...				(11.2)	(0.71)	(0.24)					
				...						2.60						
Mrk 1243	143.7	2:	0.037	1.37	17.82	1.38	-0.12	-21.80	16.0	3.55	16.50	0.85	0.23	-24.14	-24.26	4.8
			(0.01)	(0.97)	(1.03)				(3.3)	(0.16)	(0.14)					
				0.95						2.47						
NGC 5548	72.9	1	0.039	2.33	15.97	1.39	0.52	-22.94	16.3	5.66	16.13	0.94	0.21	-24.00	-24.35	13.6
			(0.01)	(0.19)	(0.17)				(0.1)	(0.10)	(0.06)					
				0.82						2.00						

TABLE 1—*Continued*

			BULGE							DISK						
Name	Dist.[a]	n_{best}[b]	e_b	r_e[c]	$\mu_e^c(K)$[d]	$(J-K)_e^c$	$(H-K)_e^c$	$M(K)_b$[e]	i[f]	r_d[c]	$\mu_d^c(K)$[d]	$(J-K)_d^c$	$(H-K)_d^c$	$M(K)_d$[e]	$M(K)_g$[e]	χ^2_ν
(1)	(2)	(3)	(4)	(5)	(6)	(7)	(8)	(9)	(10)	(11)	(12)	(13)	(14)	(15)	(16)	(17)
NGC 5940	139.4	3	···	···	···	···	···	···	46.9	6.72	17.15	···	1.20	-24.80	-24.80	3.4
			···	···	···				(16.9)	(0.45)	(0.00)					
				···						4.54						
NGC 7469	63.8	1	0.054	1.40	13.95	1.03	0.17	-23.53	45.4	4.95	15.65	0.93	0.19	-23.88	-24.47	7.3
			(0.04)	(0.08)	(0.17)				(5.2)	(0.13)	(0.05)					
				0.43						1.53						
1058+45	119.9	3:	0.305	14.20	20.15	0.68	0.15	-24.34	47.2	3.17	16.83	1.11	0.20	-23.16	-24.65	1.2
			(0.01)	(2.58)	(0.31)				(3.7)	(0.28)	(0.23)					
				8.25						1.84						
1335+39	84.7	4:	0.035	0.01	15.15	1.05	0.18	-11.82	15.5	4.16	15.89	0.91	0.23	-23.91	-23.91	2.7
			(0.01)	(557.29)	(0.01)				(1.8)	(0.04)	(0.02)					
				0.00						1.71						
Mrk 334	86.8	1	0.018	1.40	15.70	1.69	0.52	-22.48	37.1	3.90	16.67	0.78	0.12	-23.03	-23.54	1.7
			(0.06)	(0.24)	(0.29)				(7.2)	(0.18)	(0.13)					
				0.59						1.64						
Mrk 533	114.7	3	0.284	0.81	15.50	0.76	0.17	-22.68	45.4	6.38	16.55	1.02	0.30	-24.85	-24.99	12.5
			(0.01)	(0.73)	(2.16)				(9.7)	(0.34)	(0.11)					
				0.45						3.55						
Mrk 993	61.1	3	0.000	1.15	15.53	0.82	0.11	-21.98	71.8	6.94	16.58	0.93	0.22	-23.59	-23.81	2.7
			(0.05)	(0.15)	(0.22)				(3.2)	(0.14)	(0.03)					
				0.34						2.06						
NGC 3362	112.7	3:	0.009	3.09	18.45	···	0.31	-22.59	30.5	8.15	17.19	···	0.16	-24.71	-24.86	3.1
			(0.07)	(1.63)	(0.00)				(8.3)	(0.55)	(0.00)					
				1.69						4.45						
NGC 7682	66.4	3	0.000	4.13	17.65	0.92	0.19	-22.82	70.6	8.07	17.83	0.93	0.18	-22.85	-23.59	21.7
			(0.06)	(0.76)	(0.22)				(21.3)	(0.80)	(0.18)					
				1.33						2.60						

TABLE 1—*Continued*

			BULGE							DISK						
Name	Dist.[a]	n_{best}[b]	e_b	r_e[c]	$\mu_e^c(K)$[d]	$(J-K)_e^c$	$(H-K)_e^c$	$M(K)_b$[e]	i[f]	r_d[c]	$\mu_d^c(K)$[d]	$(J-K)_d^c$	$(H-K)_d^c$	$M(K)_d$[e]	$M(K)_g$[e]	χ^2_ν
(1)	(2)	(3)	(4)	(5)	(6)	(7)	(8)	(9)	(10)	(11)	(12)	(13)	(14)	(15)	(16)	(17)
Mrk 31	106.9	4:	0.000	1.86	17.84	0.87	-0.04	-22.14	71.4	10.37	19.39	0.77	0.25	-22.92	-23.35	1.5
			(0.06)	(0.51)	(0.45)				(18.8)	(1.23)	(0.14)					
				0.96						5.37						
Mrk 307	73.6	2	0.000	2.09	16.89	0.96	0.25	-22.12	...	...	...	...	...	...	-22.12	18.2
			(0.07)	(0.31)	(0.28)				...	...	...					
				0.75						...						
Mrk 545	59.9	1	0.458	2.59	15.03	0.95	0.09	-23.66	59.1	10.29	16.56	1.15	0.33	-24.43	-24.87	18.7
			(0.01)	(0.21)	(0.09)				(6.8)	(1.34)	(0.18)					
				0.75						2.99						
Mrk 575	70.8	1	0.231	1.50	16.32	1.06	0.17	-21.56	63.7	7.24	17.07	1.00	0.28	-23.53	-23.69	5.5
			(0.06)	(0.24)	(0.30)				(8.1)	(0.36)	(0.09)					
				0.51						2.49						
Mrk 717	87.2	1	0.067	1.37	15.07	1.01	0.24	-23.07	47.4	6.36	17.52	0.87	0.13	-23.25	-23.92	4.9
			(0.01)	(0.02)	(0.02)				(7.1)	(0.21)	(0.06)					
				0.58						2.69						
Mrk 719	125.5	1:	0.303	2.32	17.26	...	...	-22.74	44.6	4.65	18.28	...	...	-22.53	-23.39	1.0
			(0.01)	(0.13)	(0.24)				(5.7)	(0.42)	(0.06)					
				1.41						2.83						
Mrk 912	63.6	1	0.414	2.11	15.64	1.11	0.31	-22.74	52.6	6.18	16.60	0.84	0.21	-23.42	-23.88	1.5
			(0.01)	(0.07)	(0.04)				(2.3)	(0.10)	(0.07)					
				0.65						1.91						

[a]Distances are calculated according to the precepts of Third Reference Catalogue of Bright Galaxies (RC3) with $H_0 = 75$ kms^{-1} Mpc^{-1}.

[b]Colon signifies ill-determined; see text.

[c]Scale lengths are given in arcsec (first line, with uncertainties on the second line), and in kpc (third line).

[d]Surface brightnesses have been corrected for Galactic extinction and redshift as in Paper I, and transformed to face-on values assuming optical transparency (see MGH1); the corrected values (given in magarcsec^{-2}) are denoted by a c superscript [e.g., $\mu_e^c(K)$].

[e]In absolute K magnitudes.

[f]In degrees.